MODELING AND SIMULATION OF CORONARY STENTS:

INTRAVASCULAR DRUG DELIVERY AND ARTERIAL DRUG DISTRIBUTION

BY

XIAOXIANG ZHU

THESIS

Submitted in partial fulfillment of the requirements
for the degree of Master of Science in Chemical Engineering
in the Graduate College of the
University of Illinois at Urbana-Champaign, 2010

Urbana, Illinois

Advisor:

Professor Richard D. Braatz

ABSTRACT

In-stent restenosis still occurs in coronary arteries implanted with drug-eluting stents, with the maximum thickness observed at the vascular site of maximum inter-strut angle. This phenomenon may be related to the specific spatiotemporal drug uptake in the arterial wall. In this work local delivery of a hydrophobic drug from a drug-eluting stent implanted in a coronary artery is investigated using a mathematical model that couples drug diffusion and reversible binding in the arterial wall. The model is solved by the finite volume method with varied stent-coating and vascular diffusivities for (*i*) drug loading at concentrations less than or equal to the solubility, and (*ii*) high drug loading at concentrations greater than the solubility. Drug release profiles in the coating are observed to depend not only on the coating diffusivity but also on the properties of the surrounding arterial wall. Distinguished dependence on the vascular diffusivity and coating diffusivity of the spatially-averaged drug levels in the wall at quasi-steady state are discussed. Anisotropic drug diffusivities result in similar average drug levels in the arterial wall but very different spatial distributions. Higher circumferential vascular diffusivity results in more uniform drug loading in the upper layers and is potentially beneficial in reducing in-stent restenosis. An analytical expression is derived for determining whether higher free-drug concentration than that of bound-drug can occur in the arterial wall.

Keywords: drug-eluting stents, hydrophobic drug, mathematical modeling, intravascular delivery, restenosis, reversible binding

To My Family

ACKNOWLEDGMENTS

Great thanks to my advisor, Professor Richard D. Braatz, for the guidance on the research and my life. I am also thankful to all my labmates for their inspiring discussions and the fun times we enjoyed as a group. I am extremely grateful to my parents, my family, and my friends who have been with me along the way, always offering support and love. This work was possible through the support from the National Institutes of Health NIBIB 5RO1EB005181 and the National Science Foundation (Grant #0426328).

TABLE OF CONTENTS

CHAPTER 1

INTRODUCTION

Drug-eluting stents have shown great improvement in reducing In-Stent Restenosis after angioplasty procedures compared with bare metal stents [1-4]. The device enables a prolonged local delivery of active drugs, such as sirolimus or paclitaxel, which are embedded in and released from the polymeric stent-coating and can interrupt certain stages in in-stent restenosis formation [5-7]. Great efforts have been carried out towards stent design [8], *in vitro* drug release from polymeric stent-coating [9-13] (with various configurations including but not limited to drug type and loading, polymer type and molecular weight, coating thickness), drug physiochemical and physiological properties [7, 14-16], *in vivo* examination of drug delivery and arterial drug uptake [15, 17-21], and in-stent restenosis formation [22-26]. Nevertheless, the *in vivo* study of drug-eluting stents is limited by factors such as huge time requirement and the complexity and difficulty in measurement and quantification.

Modeling and simulation offers an alternative approach for drug-eluting stents study and can improve our understanding of *in vivo* drug-eluting stent functions. Drug release from coating and drug-vascular tissue interactions were studied in one-dimensional models [27-29]. Analytical solution for drug diffusion in one-dimensional multi-layer wall structure was also derived [30]. Convective and diffusive transports of drug in the arterial wall were assessed for both hydrophilic and hydrophobic drugs [31, 32]. Impact of thrombus [33], blood flow [34, 35], stent coating [36], and strut position [37] on stent-based drug delivery was investigated by studying a single strut in an axial

cross-section of the artery using a coupled computational fluid dynamics and mass transfer model. In a radical cross-section model, drug elution from a fully embedded stent strut was found to be most effective with a bi-layer gel paved stent [38]. Multiple struts models were also developed to study the impact of different strut configurations (half, fully, and not-embedded) and diffusivities [39-41] on arterial drug up-take. Mechanics and fluid dynamics simulation has also been done to study stent expansion and interaction with coronary artery [42]. Wall stress distributions after insertion and deployment were compared by simulation for three different stent designs [43].

It is reported that in-stent restenosis is more likely to happen in stented coronary arteries with non-uniformly distributed struts, with the maximum thickness of neointimal hyperplasia occurring at the site with maximum inter-strut angle [23]. In order to understand this problem from the perspective of arterial drug-uptake, this work mathematically models the delivery of a hydrophobic drug from a drug-eluting stent with bio-durable polymeric coating into the arterial wall and incorporates drug release kinetics, physiological behavior, and stent geometry. The local drug delivery and distribution is studied in a detailed manner for implications on reducing in-stent restenosis for drug-eluting stents. The long-term objective of our research is to develop mathematical models for the *in vivo* release in the arterial wall from drug-eluting stents, which someday can be used for optimal stent design *in silico* instead of implanting sub-optimal stents into patients and waiting to observe undesirable outcomes.

CHAPTER 2

MODEL STRATEGY FOR DRUG-ELUTING STENTS

2.1 Description of an Implanted Stent

The type of drug-eluting stent studied in this paper has a bio-durable polymeric coating that delivers a hydrophobic drug. This is the case for FDA-approved stents such as Cypher stent (Cordis, Johnson & Johnson) and Taxus stent (Boston Scientific). The cross-sectional view of the coronary artery with an implanted eight-strut stent [31] is illustrated in Figure 1a. Square shape of struts is used with strut dimension a having a typical value from Cypher Stents [8,24,42]. The struts are assumed to be distributed evenly in the lumen with same degree of embedment in the arterial wall.

Due to symmetry, the model domain can be reduced to a single strut section (indicated by dotted lines in Figure 1a.). Considering that the thickness of the arterial wall (L_x, ~200μm [28-29,44]) is small compared to the diameter of the lumen (2.5~3.5 mm [10,39,40]), the single strut section is accurately modeled as a rectangular arterial wall domain, as in Figure 1b. The inter-strut distance (distance between the centers of two adjacent struts), L_y, is estimated for an eight-strut stent in a 3 mm coronary artery. The transmural and circumferential directions are labeled as the x and y axis, respectively. Blood flow has a direction into the paper plane. Parameters defining the spatial dimensions are labeled in Figure 1b, with their values summarized in Table 1. The coating thickness δ has values in the literature within the range of 10~100 μm [24,39, 40], and a value of 50 μm is used [39,40]. Strut embedment in the wall can range from no embedment to fully-embedded [39-41], revealing slightly different uniformity in drug

distribution and higher amount of drug in the arterial wall with increased degree of embedment. In this work the depth of strut embedment into the wall L_p is used with a value close to half-embedment.

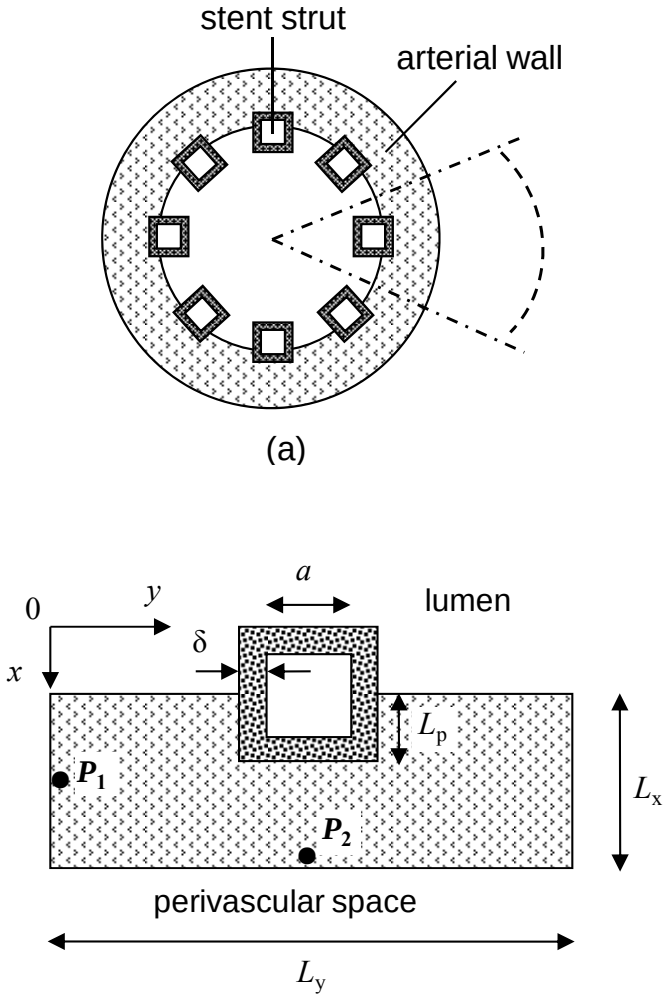

Figure 1. (a) Cross-sectional view of a stented vessel. Dashed lines show a reduced domain by symmetry. (b) Extracted rectangular vascular domain with partial embedment of a single stent strut.

Table 1. Dimensions and Model Parameters

Dimensions		
strut dimension	a	140 μm [8,24,42]
coating thickness	δ	50 μm [39,40]
strut embedment	L_P	zero ~ total embedment [39-41]
arterial wall thickness	L_x	200 μm [28,29,44]
inter-strut distance	L_y	1000 μm
Model parameters		
initial binding site level	S_0	10^{-5} M [14]
initial drug level in the coating	C_0	10^{-5} M [29]
drug solubility in the coating	C_s	10^{-5} M
drug diffusivity in the coating	D_1	0.01~1 $\mu m^2/s$ [29,39]
isotropic drug diffusivity in the wall	D_2	0.1~10 $\mu m^2/s$[14,15,29,39]
transmural diffusivity in the wall	D_{2x}	0.1~10 $\mu m^2/s$
circumferential diffusivity in the wall	D_{2y}	1~100 D_{2x} [14, 17]
resistance at perivascular boundary	R_{per}	5~100 s/μm [29,31]
association rate constant (binding)	k_a	10^4 $M^{-1}s^{-1}$ [16,28,29]
dissociation rate constant (unbinding)	k_d	0.01 s^{-1} [16,28,29]
partition coefficient at the coating-arterial wall interface	κ_{CW}	1

2.2 Mathematical Model

The drug delivery proceeds via pure drug diffusion in the polymeric coating (Eq.(1), Table 2) followed by combined drug diffusion and reversible binding in the arterial wall (Eq.(2), Table 2) [14,28,29,33]. Drug transport by convection within the arterial wall is negligible compared with diffusion [35] due to low local Peclet number [21] and is absent in most models [33-34, 36]. The three drug diffusivities D_1, D_{2x}, and D_{2y} correspond to these in the coating and the transmural and circumferential directions in the arterial wall, respectively. Drug binding in the wall is approximated as a first-order reversible reaction $C + S \underset{k_d}{\overset{k_a}{\rightleftarrows}} B$ characterized by an association (binding) rate constant k_a forming bound drug (B) and a dissociation (unbinding) rate constant k_d [28,29,34]. The amount of available binding sites S at each position within the wall is tracked by the difference between the initial binding sites level S_0 and bound drug level B.

Table 2. Mathematical Representation of the Model

Model Equations		
drug in the coating	$\frac{\partial C}{\partial t} = D_1 \frac{\partial^2 C}{\partial x^2} + D_1 \frac{\partial^2 C}{\partial y^2}$	(1)
free drug in the arterial wall	$\frac{\partial C}{\partial t} = D_{2x} \frac{\partial^2 C}{\partial x^2} + D_{2y} \frac{\partial^2 C}{\partial y^2} - k_a \left(S_0 - B\right) C + k_d B$	(2)
bound drug in the arterial wall	$\frac{\partial B}{\partial t} = k_a \left(S_0 - B\right) C - k_d B$	(3)

Table 2. (cont.)

Boundary Conditions		
lumen-wall interface, lumen-coating interface, perivascular boundary	$J_{mn} = \frac{1}{R_{nm}}(C_m - \frac{C_n}{\kappa_{nm}})$	(4)
coating-strut interface, Left/right wall boundary	$J = 0$	(5)
coating-wall interface	$\kappa_{cw} C_{wall} = C_{coating}$	(6)
	$J_{wall} = J_{coating}$	(7)

Initial Conditions (*t = 0*)			
In the coating	$C = C_0$	In the arterial wall	$C = 0$
	$B = 0$		$B = 0$

The boundary conditions are expressed in flux form at each interface in Table 2. Eq.(4) describes the flux J_{mn} at an interface between domains *m* and *n* by a mass transfer resistance R_{nm} and partition coefficient κ_{nm} [31,32],

$$\kappa_{nm} = [C_n / C_m]_{equilibrium} \tag{8}$$

For example, at lumen-arterial wall interface, the flux is

$$J_{LW} = \frac{1}{R_{LW}}(C_L - \frac{C_W}{\kappa_{WL}}) \tag{9}$$

which is expressed in terms of the lumen drug level C_L, the drug level in the arterial wallC_W, the partition coefficient $\kappa_{WL} = [C_W / C_L]_{equilibrium}$ and the resistance R_{WL}. Similar boundary conditions are also used for lumen-coating interface and perivascular boundary.

At interfaces with the lumen, drug entering the blood are presumed to be washed out, and $C_L = 0$ [28,29,31]. Zero drug concentration in the perivascular space, $C_P = 0$, is also used [29,31]. For hydrophobic drug like sirolimus and paclitaxel, the partition coefficients are very high ($\kappa_{wl} >> 1$) [14,15,18,32] and drug partitioning into the arterial wall is strongly favored. This and a high resistance imposed by the intimal [20,21] can greatly damp the drug depletion into the blood and result in a negligible drug flux into the lumen.

Zero flux boundary condition Eq. (5) applies to the other interfaces including the coating-strut interface (physical isolation) and right/left wall boundaries (due to symmetry). The boundary conditions at the wall-coating interface are described by concentration partitioning (zero resistance) (Eq. (6)) and flux matching (Eq. (7)).

2.3 Dimensional Analysis

Some insights of the system characteristics can be obtained from dimensional analysis. The characteristic lengths of the coating domain and wall domain are the coating thickness δ and lengths L_x and $L_y/2$, respectively. Define $\overline{C} = C/C_0$, $\overline{B} = B/S_0$, and non-dimensionalizeEqs. (1)-(3) to obtain Eqs. (10)-(12) in Table 3.

Three characteristic time scales appear, τ_1, τ_2, τ_3, corresponding to diffusion in the coating, transmural diffusion, and the binding reaction. An evaluation of the magnitude

of the three groups gives $\tau_1 \sim 10^3$-10^5 s, $\tau_2 \sim 10^3$-10^5 s, and $\tau_3 \sim 10^2$ s, which indicate that reversible binding is very fast compared to diffusion.

Table 3. Non-dimensionalized Equations

$$\frac{\partial \overline{C}}{\partial (t/\tau_1)} = \frac{\partial^2 \overline{C}}{\partial (x/\delta)^2} + \frac{\partial^2 \overline{C}}{\partial (y/\delta)^2} \tag{10}$$

$$\frac{\partial \overline{C}}{\partial (t/\tau_2)} = \frac{\partial^2 \overline{C}}{\partial (x/L_x)^2} + G_1 \frac{\partial^2 \overline{C}}{\partial (2y/L_y)^2} - G_2 \left(1-\overline{B}\right)\overline{C} + G_3 \overline{B} \tag{11}$$

$$\frac{\partial \overline{B}}{\partial (t/\tau_3)} = \frac{G_2}{G_3}\left(1-\overline{B}\right)\overline{C} - \overline{B} \tag{12}$$

Characteristic time scales and dimensionless groups

$\tau_1 = \delta^2/D_1$	$\tau_2 = L_x^2/D_{2x}$	$\tau_3 = 1/k_d$
$G_1 = \dfrac{L_x^2/D_{2x}}{L_y^2/4D_{2y}}$	$G_2 = \dfrac{L_x^2}{D_{2x}} k_a S_0$	$G_3 = \dfrac{L_x^2}{D_{2x}} \dfrac{k_d S_0}{C_0}$

The significance of diffusion and reversible binding in the wall are also implied by their corresponding dimensionless groups in Eq. (11). Compared with the coefficient of transmural diffusion component (which is 1), the reaction components have very large coefficients, $G_2 \sim 10^2$-10^4 and $G_3 \sim 10^1$-10^3, which also implies that the binding reactions play a very strong role in the spatiotemporal dynamics. The competition between association and dissociation reactions is quantified by $G_2/G_3 \sim 10$ in Eq. (12). Larger values for this ratio indicate a preference of association over dissociation.

The competition between diffusion in the transmural and circumferential directions is implied by the dimensionless group G_1. With increasing D_{2y}, the group G_1 increases from ~0.1 to ~10, revealing an increasing importance of circumferential diffusion in Eq. (11) compared with transmural diffusion.

2.4 Numerical Simulation

The mathematical model in Table 2 was simulated using the finite volume method. To illustrate, for a cell centered at (x,y) in a mesh with cell size Δx by Δy, Eq. (2) can be expressed as

$$\begin{aligned}\frac{d}{dt}\int_{x-\frac{\Delta x}{2}}^{x+\frac{\Delta x}{2}}\int_{y-\frac{\Delta y}{2}}^{y+\frac{\Delta y}{2}} C(x,y,t)dxdy &= J_x\Big|_{x-\frac{\Delta x}{2},y}\Delta y - J_x\Big|_{x+\frac{\Delta x}{2},y}\Delta y + J_y\Big|_{x,y-\frac{\Delta y}{2}}\Delta x - J_y\Big|_{x,y+\frac{\Delta y}{2}}\Delta x \\ &- k_a\int_{x-\frac{\Delta x}{2}}^{x+\frac{\Delta x}{2}}\int_{y-\frac{\Delta y}{2}}^{y+\frac{\Delta y}{2}}\left(S_0 - B(x,y,t)\right)C(x,y,t)dxdy + k_d\int_{x-\frac{\Delta x}{2}}^{x+\frac{\Delta x}{2}}\int_{y-\frac{\Delta y}{2}}^{y+\frac{\Delta y}{2}} B(x,y,t)dxdy\end{aligned} \tag{13}$$

Where J_x, J_y correspond to the fluxes in x,y directions, respectively.

Applying a forward-difference approximation of the time derivative with a time step Δt and mesh size $h = \Delta x = \Delta y$ results in

$$\begin{aligned}\frac{\overline{C}_{i,j}^{n+1} - \overline{C}_{i,j}^{n}}{\Delta t} &= \frac{1}{h}\left(J_x\Big|_{i-h/2,j}^{n} - J_x\Big|_{i+h/2,j}^{n} + J_y\Big|_{i,j-h/2}^{n} - J_y\Big|_{i,j+h/2}^{n}\right) \\ &- k_a\left(S_0 - \overline{B}_{i,j}^{n}\right)\overline{C}_{i,j}^{n} + k_d\overline{B}_{i,j}^{n}\end{aligned} \tag{14}$$

where superscript n is the index for the time level, subscripts i, j are the indices for x and y, $\pm h/2$ indicates the position of the boundaries with neighboring mesh cells, and $\overline{C}$ and $\overline{B}$

are the average of the free and bound drug levels over the mesh cell centered at (i,j) at time index n. Flux across boundary of two adjacent mesh cells was calculated by the second-order centered difference, *i.e.*

$$J_x\Big|_{i-h/2,j}^{n} = -D\frac{\overline{C}_{i,j}^{n} - \overline{C}_{i-1,j}^{n}}{h} \tag{15}$$

The numerical simulations were implemented in Matlab 2008 running on an Intel-based personal computer. Values of parameters used in the simulation are summarized in Table 1. For drug diffusion in the arterial wall, isotropic drug diffusivity (D_2) was first investigated, followed by an anisotropic diffusivity study. A range of 0.1~10 $\mu m^2/s$ of the transmural diffusivity is investigated [14,15,29,39], while the circumferential diffusivity can be the same for large drug molecules or one or two orders of magnitude larger for small drugs [14,17]. Reported values are chosen for the association (dissociation) rate constants k_a (k_d) [16,28,29], binding site concentrations (S_0) [14], as well as the resistance at perivascular interface(R) [29,31]. The partition coefficient at coating-wall interface was assumed as one.

Initial conditions for simulation are summarized in Table 2, which indicates uniformly dispersed drug in the polymer coating at concentration C_0. The binding sites are evenly distributed throughout the arterial wall at concentration S_0 initially.

CHAPTER 3

SIMULATION RESULTS AND DISCUSSION

3.1 Low Initial Drug Load in the Coating ($C_0 \leq C_s$)

The drug is completely dissolved in the polymer matrix when the loading is equal to or less than the solubility, and the drug transport in the coating is purely diffusion controlled [45]. Due to the absence of drug aggregates, the dissolved drug concentration in the stent coating decreases gradually with the release.

3.1.1 Release Profile in the Stent Coating

The release rate decreases significantly with reduced diffusivity in the stent coating, D_1, when the isotropic diffusivity in the wall D_2 remains constant (see Figure 2). Within the simulated range, almost all the drug is released in the first 200 hr at a high coating diffusivity D_1 of 1 $\mu m^2/s$, while a two-order lower D_1 ensures a prolonged release of the drug by releasing about 60% within 400 hr. Lower coating diffusivity is associated with prolonged drug release, and this is in agreement with previous findings [36,39].

Moreover, changes in the vascular diffusivity D_2 and the presence of binding in the wall both affect the drug release process. Increment of an order in the magnitude of D_2 significantly enhances the release rate as well, compared to the same change in D_1. Elimination of the binding reactions results in a slightly reduced release rate, explained by the fact that with binding a greater concentration gradient is produced in the wall by transferring free drug into bound form [29], and thus faster drug transport from the

coating-wall interface. While the coating diffusivity is mainly investigated for drug release kinetics study, these findings imply that the release profile is under a combined influence of diffusion in both the coating and the arterial wall and binding interactions. Under such circumstance, standard *in vitro* measurement carried out in buffer solutions is not always a close representation of the *in vivo* drug release. In particular, for a drug-eluting stent with hydrophobic drug, where the drug dissipation into blood is small or negligible, drug-vascular tissue interactions play a significant role and can vary the release profiles greatly.

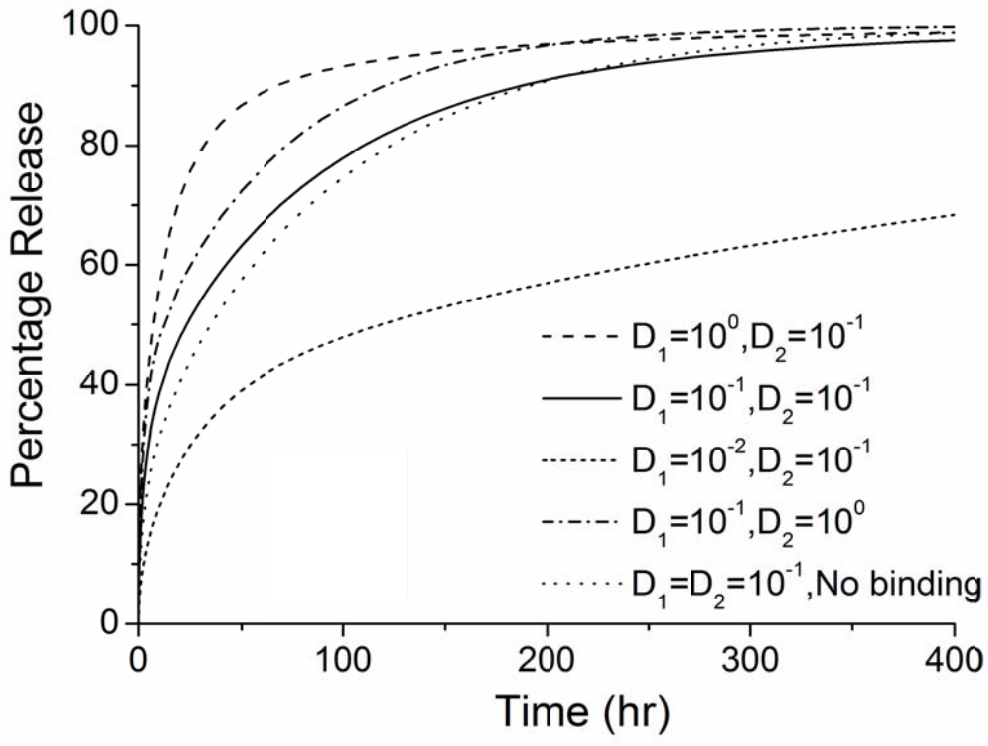

Figure 2. Drug release profiles in the stent coating at different diffusivities (with binding) and in non-binding case. The diffusivities are in units of $\mu m^2/s$.

3.1.2 Spatially-Averaged Drug Concentration

The temporal profiles for the spatial average of the bound- and free-drug concentrations in the arterial wall were computed (that is, the integral of the concentration over the wall domain in Figure 1 divided by its volume). The spatially-averaged bound-drug concentration was about an order of magnitude higher than that of free drug in Figure 3, indicative of the preferred association than dissociation in the reversible binding, consistent in magnitude with the ratio of their dimensional groups, $G_2/G_3 = 10$. For each simulated diffusivity pair (D_1, D_2), the spatially-averaged bound- and free-drug concentrations have similar trends over time.

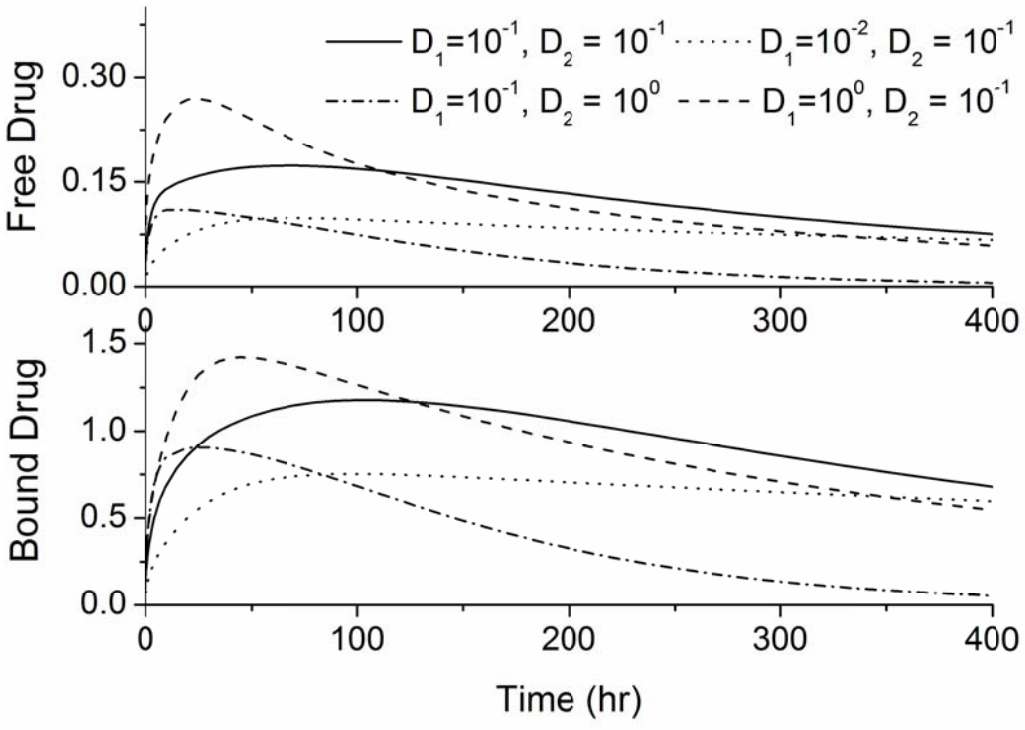

Figure 3. Spatially-averaged concentrations for the free and bound drug in the arterial wall for various coating and vascular diffusivities ($\tau_2 = 33.6$ hr for $D_2 = 0.1$ and the diffusivities are in units of $\mu m^2/s$).

The spatially-averaged free- and bound-drug concentrations in the arterial wall approach quasi-steady values that reduce slowly for most (D_1, D_2) pairs (see Figure 3). The time needed to reach quasi-steady states is estimated by the transmural diffusion time scale τ_2, around which both the free- and bound-drug levels also reach their peaks. An evaluation of the characteristic time constants with the real dimensions (reduced transmural distance due to strut embedment) in Figure 1b gives τ_2 = 33.6 hour for D_2 = 0.1 $\mu m^2/s$. This is in agreement with the peak positions for corresponding plots in Figure 3. Besides, noticeably the quasi-steady spatially-averaged drug concentrations are dominated by the diffusivity in the wall, D_2, rather than the diffusivity through the stent coating, D_1. While all three (D_1, D_2) pairs with the same D_2 (0.1 $\mu m^2/s$) achieved similar quasi-steady spatially-averaged drug concentrations, the fourth (D_1, D_2) pair with an order-of-magnitude higher D_2 (1 $\mu m^2/s$) had a much lower quasi-steady drug level (see Figure 3). Under quasi-steady conditions, both diffusion and binding achieve a dynamic equilibrium throughout the arterial wall, and with the drug dissipation in the arterial wall occurring through the perivascular space, the binding kinetics and the diffusivity D_2 provide the tradeoff that specifies the quasi-steady spatially-averaged drug concentrations. Higher diffusivity in the wall speeds the transport of free drug through the arterial wall and faster dissipation of drug at the interface of wall-perivascular space.

While the quasi-steady spatially-averaged drug concentrations are similar for the same vascular diffusivity D_2, the spatially-averaged drug concentrations are higher in early times for increased stent coating diffusivity D_1 (see Figure 3). The higher D_1 results in faster initial drug transport through the stent coating into the arterial wall, before approaching quasi-steady spatially-averaged drug concentrations. These observations

provide guidance in the design of the stent coating to maintain the drug concentrations in the arterial wall within the therapeutic window throughout the treatment.

3.1.3 Anisotropic Diffusivities in the Wall

The drug diffusivity in the transmural and circumferential directions tend to be anisotropic due to the arterial ultra-structure, mainly attributed by the flat shape of the smooth muscle cells [14,17]. For small drug molecules, the circumferential diffusivity can be orders of magnitude larger than that in the transmural direction, but the anisotropy in the diffusivity gradually diminishes with increasing drug molecules [14,17]. Although anisotropic diffusivity was accounted in some of the studies [31,40], there has not been a full investigation on this property. In this part of the study, diffusivity anisotropy in the arterial wall is studies detail for its impact on the drug level and distribution in the wall.

The spatially-averaged drug concentrations in the arterial wall were enhanced with increased circumferential diffusivity, D_{2y} (see Figure 4). With increased D_{2y}, the diffusion in the circumferential direction competes over penetration through the arterial wall, reduces the penetrated drug concentration close to the perivascular interface and corresponding local drug dissipation. Meanwhile, increased vascular diffusivity in the circumferential direction more quickly transports drug in the arterial wall away from the stent coating, resulting in faster drug release from the stent coating. These two factors contribute to the enhanced spatially-averaged bound-drug concentrations at increased D_{2y}. In early times the spatially-averaged free-drug concentration is slightly lower at enhanced circumferential diffusivity due to the increased availability of binding sites within the arterial wall in which drug has diffused. With the anisotropy ratio (ratio of

circumferential diffusivity to transmural diffusivity, D_{2y}/D_{2x}) increased from 10 to 100, the corresponding increment in the pseudo-steady drug levels becomes less significant. This is partly explained as that the circumferential diffusion is very fast compared with transmural penetration, and the latter becomes the dominant diffusion limitation for drug transport in the wall and dissipation at the perivascular side. More details are included in following discussions for Figure 5.

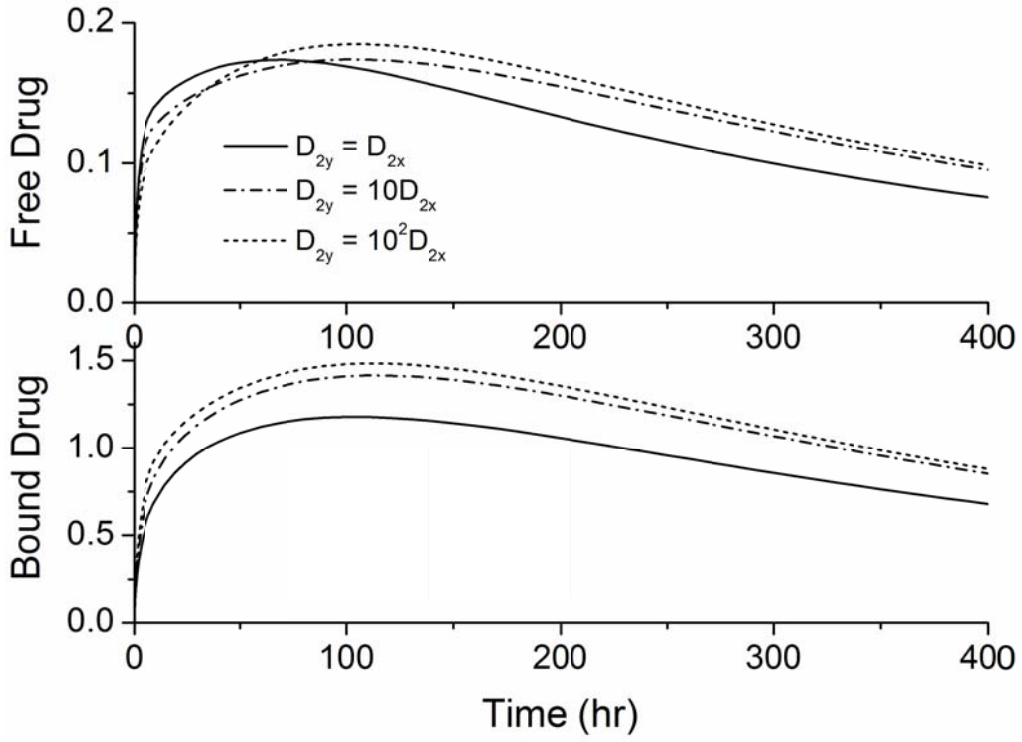

Figure 4. Spatially-averaged concentrations for the free and bound drug in the arterial wall at various circumferential diffusivities (D_{2x} = 0.1 μm^2/s).

Anisotropic diffusivity has a very large effect on the spatial distribution of drug in the arterial wall (see left column of Figure 5). Depending on the particular value for the circumferential diffusivity D_{2y}, drug concentrations can range from being highly non-uniform along the circumference of the arterial wall (Figure 5. A-1) to extremely uniform

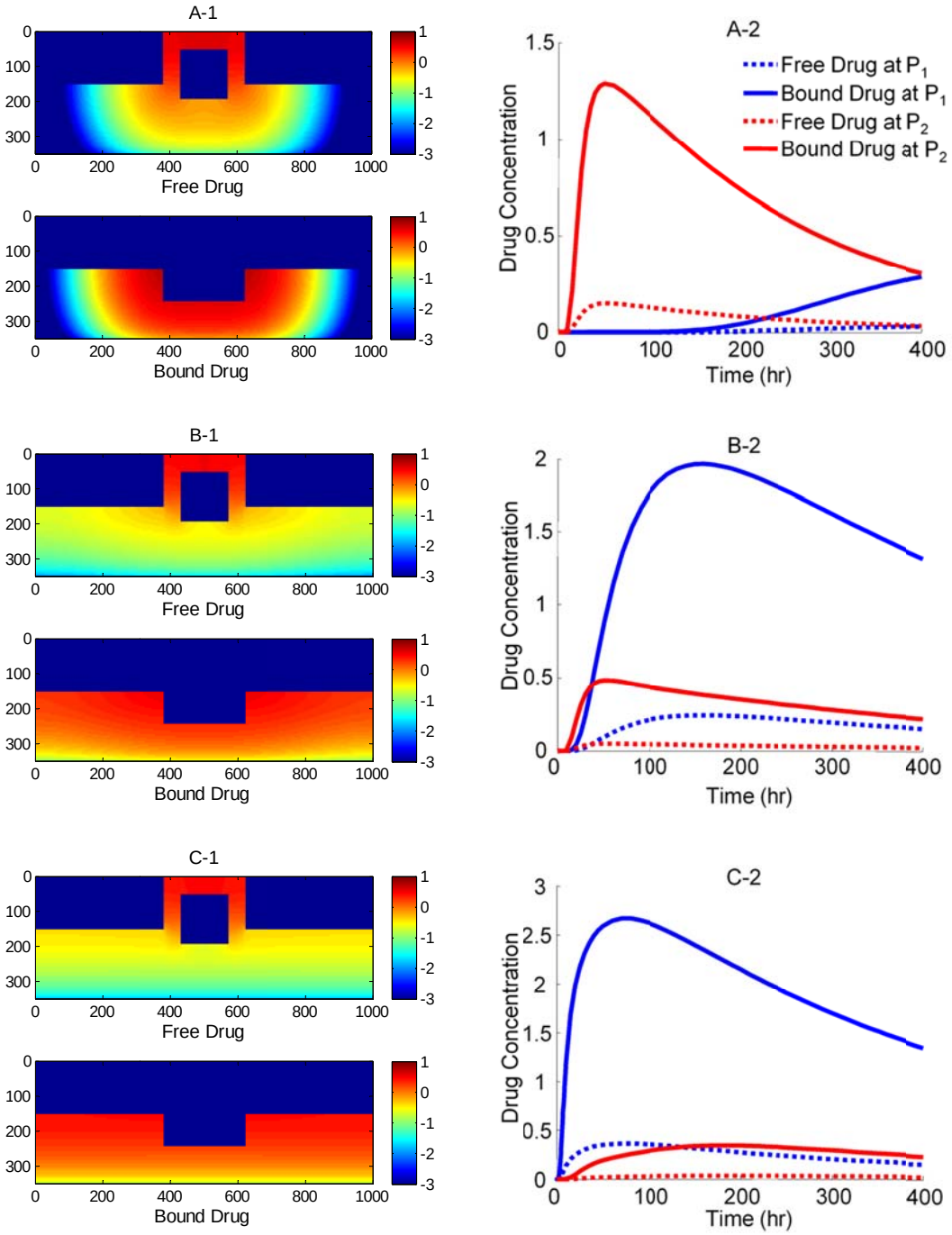

Figure 5. Left column: drug concentration fields at different circumferential diffusivities at 100 hr with low drug loading in the coating (logarithmic plots, D_{2x} = 0.1 μm^2/s); Right column: time evolution of drug concentrations at point P_1 (blue) and point P_2 (red), free (--) and bound (—) drug. (A) $D_{2y} = D_{2x}$, (B) $D_{2y} = 10D_{2x}$, (C) $D_{2y} = 100D_{2x}$.

(Figure 5. C-1), whereas a concentration gradient always exists in the transmural direction. At very high circumferential diffusivity, the drug concentrations are well approximated as only being a function of time and depth in the transmural direction.

The time evolution of the drug concentrations at positions P_1 and P_2 (near the left and the perivascular boundaries in Figure 1b) are shown in the right column of Figure 5. With increasing circumferential diffusivity D_{2y}, the free- and bound-drug concentrations at P_1 massively increase, and those at P_2 decrease. At increased D_{2y}, drug dissipation at the perivascular boundary is reduced with the reduced local drug concentrations, resulting in the higher spatially-average drug concentrations observed in Figure 4.

The first appearance of drug at P_1 and P_2 corresponds to the diffusion time in each direction (see right column in Figure 5). For isotropic diffusion in Figure 5A-2, the diffusion time in the circumferential direction (~180 hr) is almost 12 times as long as the penetration time (~15 hr). The drug distribution is very non-uniform in the circumferential direction when transmural penetration is well established, and areas with negligible drug concentrations exist far away from the strut (see Figure 5A-1). Similar qualitative results have been reported in which drug binding was absent [31]. The lack of drug in upper layers far away from the strut in the circumferential direction can be a serious factor of restenosis occurrence, as it is known that high drug concentrations in the upper layers of wall is more important than penetration in suppressing restenosis [7]. Lack of drug in the upper layers of the arterial wall during the early days after implantation provides a potential explanation to the clinical observation that the thickest restenosis occurs at the largest inter-strut angle area when the struts are unevenly placed

[23]. In addition, this provides an alternative factor to the observed asymmetric cross-sectional neointimal thickness distribution, for which lower wall shear stress was considered as an important factor to induce more neointimal growth [25,26].

For $D_{2y} = 10D_{2x}$, the time evolution of the free- and bound-drug concentrations at the left and adventitia boundaries in Figure 5B-2 shows comparable diffusion times with both positions initially receiving drug at a similar time (~15 hrs). With even higher D_{2y} ($100D_{2x}$), the diffusion time in the circumferential direction is negligible compared to that of penetration (see Figs. 5C-1 and 5C-2). In this case, a fast coverage of drug in the upper media layers is achieved within ~2 hr, and nearly uniform drug concentrations in the circumferential direction are produced. The potential adverse effect of unevenly placed struts could be greatly reduced, compared to isotropic diffusion. These simulations indicate that drugs with high anisotropy in diffusivity in the arterial wall are preferable from the clinical point of view, in terms of achieving higher and more uniform drug level in the upper layers of the arterial wall.

3.2 High Initial Drug Load in the Coating ($C_0 >> C_s$)

In real applications high drug loadings are used that are very often orders of magnitude higher than the solubility in the matrix and most of the drug is dispersed in the polymer matrix in aggregated form [9,12].

While the drug is released from the stent coating, the dynamic equilibrium between drug aggregates and dissolved drug ensures a continuous drug supply. When the dynamic equilibrium is fast compared to the release, the drug concentration can be

assumed as constant at its solubility within the coating. This is similar to the continuum pharmacokinetics investigated in some works [31,35].

Under this circumstance, the spatially-averaged drug concentrations in the arterial wall achieve quasi-equilibrium values (as in Figure 6). The quasi-equilibrium can last until the average drug concentration in the coating is eventually reduced close to its solubility. Shorter times are required to achieve quasi-equilibrium with increased circumferential diffusivity, and the quasi-equilibrium drug levels are enhanced. Due to the availability of the abundant drug source in the coating, the trend of enhancement is more significant here than in Figure 4.

The drug distribution profiles for isotropic diffusivity indicate that quasi-equilibrium has not yet fully established in 400 hours due to the slow diffusion in the circumferential direction (Figure 7A-1, 2). The low quasi-equilibrium drug levels at sites far away from the strut in the circumferential direction again justifies the finding in Section 3.1.3 that maximum restenosis thickness at maximum inter-strut angle is related to lack of drug in that position.

Quasi-equilibrium was established quickly when the circumferential diffusivity D_{2y} is enhanced (cases B and C in Figure 7.). In plot B-1, the free-drug concentration forms a clear gradient centered at the strut even at quasi-equilibrium, indicating a non-uniform drug level in both circumferential and transmural directions. When D_{2y} is increased to 2 orders in magnitude as large as D_{2x} in Figure 7. C-1, the fast circumferential diffusion compared with penetration resulted in planar layers containing

uniform equilibrium drug level, and layers form a drug gradient downward the arterial wall, similar to Figure 5C-1.

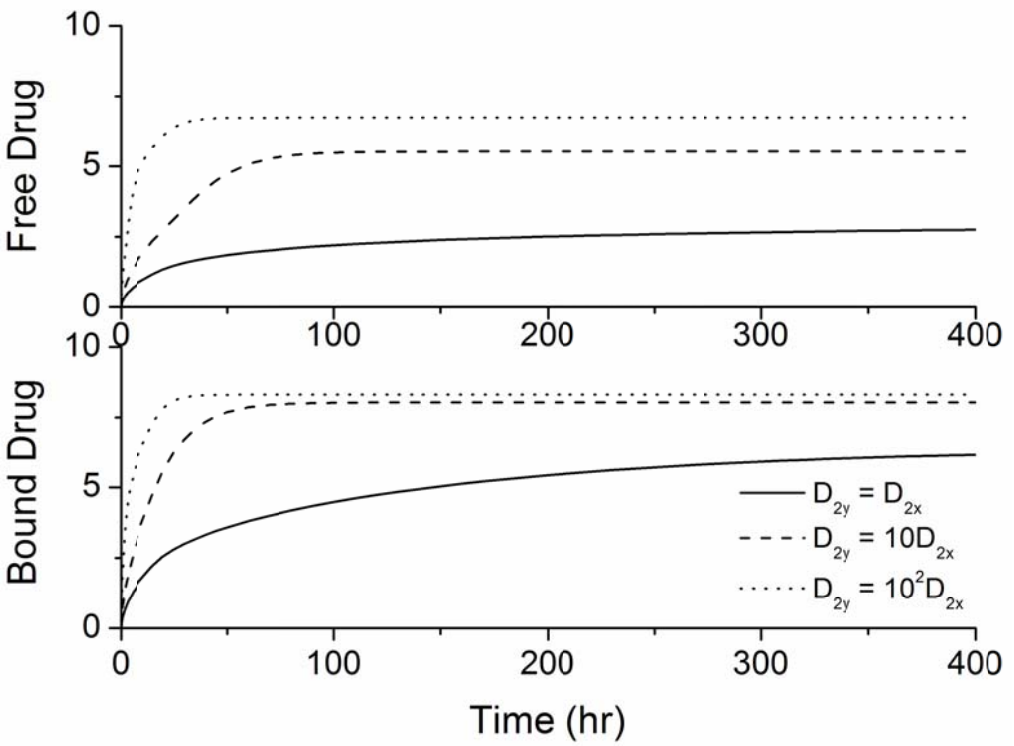

Figure 6. Spatially-averaged free- and bound-drug concentrations in the arterial wall under continuous drug release from the stent coating at high drug loading (D_{2x} = 0.1 $\mu m^2/s$).

The concentrations at boundary points P_1 and P_2 (as located in Figure 1.b) in the right column of Figure 7 have a similar initial trend as those in Figure 5, but reach at constant quasi-equilibrium levels. In Figure 7.C-2, the free-drug concentration at quasi-equilibrium is higher than that of the bound drug at P_1. A careful investigation of C-1 shows that this circumstance is true for a large vascular area neighboring the strut.

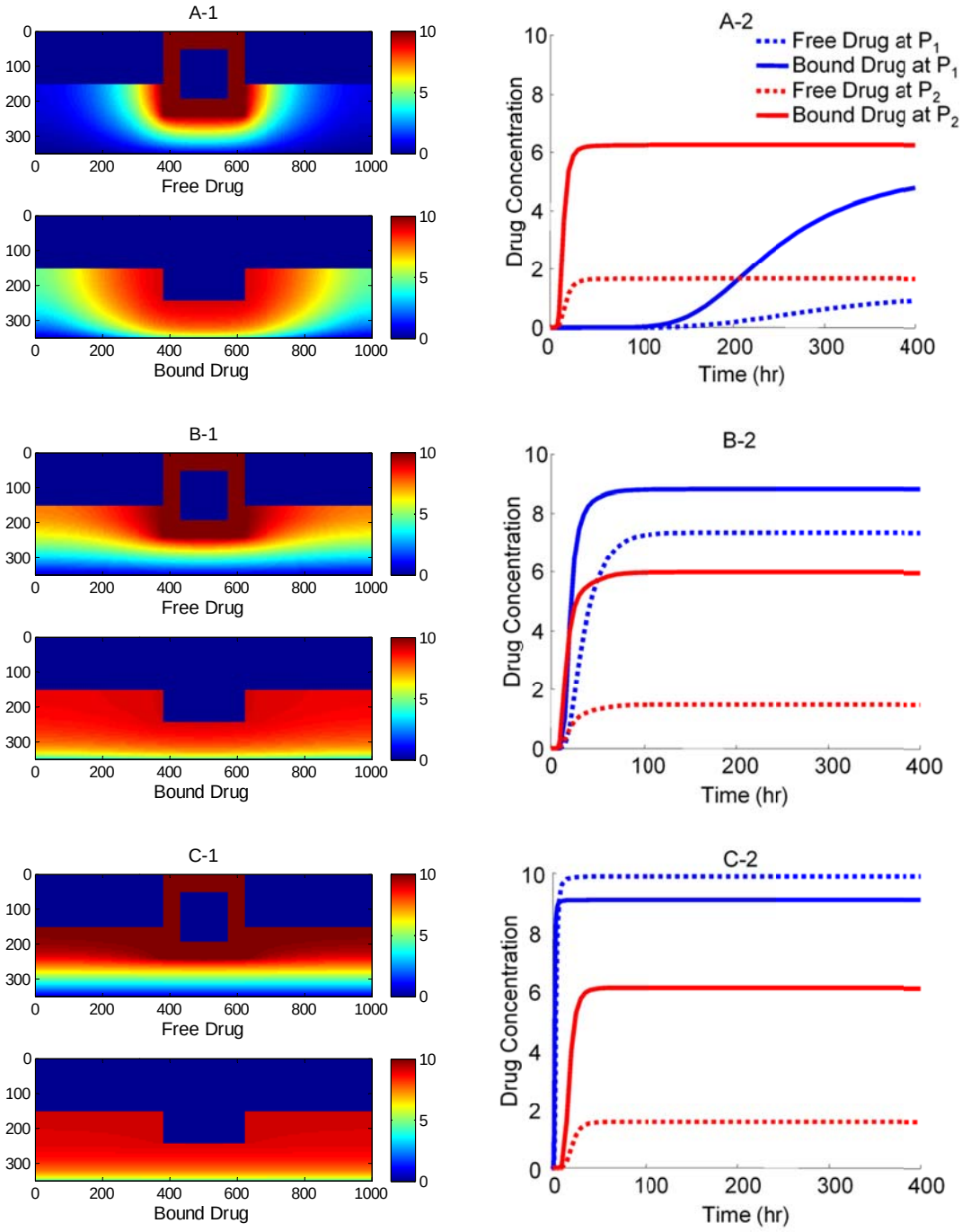

Figure 7. Left column: drug distribution profiles at different circumferential diffusivities at 400 hr with high drug loading in the coating (D_{2x} = 0.1 μm^2/s); Right column: drug concentration evolution at point P_1 (blue) and point P_2 (red), free (--) and bound (—) drug. (A) $D_{2y} = D_{2x}$, (B) $D_{2y} = 10D_{2x}$, (C) $D_{2y} = 100D_{2x}$.

Although part of the arterial wall has higher free-drug level than that of bound drug, the spatially-averaged concentration is still lower for free drug (see Figure 6). These simulations show that, while the spatially-averaged concentrations have higher bound-drug concentration than that of free drug, as expected from $G_2/G_3 = 10$, this does not necessarily hold for individual vascular sites.

The critical condition for the circumstance that free-drug concentration exceeds that of bound-drug can be derived. At equilibrium conditions, the rates of association and dissociation in Eq. (3) are equal,

$$k_a C(S_0 - B) = k_d B \tag{16}$$

This equation can be rearranged to solve for the free-binding-site concentration in terms of the free-drug concentration,

$$B = KCS_0 / \left(KC + 1\right) \tag{17}$$

where $K = k_a/k_d$ is the equilibrium binding constant.

To acquire a higher concentration of free drug than bound drug, or $C > B$, the condition can be combined with Eq. (17) to give

$$C > S_0 - 1/K \tag{18}$$

The highest free-drug concentration in the wall occurs at the coating-wall boundary, where $C = C_s / \kappa_{CW}$, and the inequality becomes

$$C_s/\kappa_{CW} > S_0 - 1/K \tag{19}$$

When this inequality is satisfied, higher free-drug concentration can occur in the region close enough to the strut. The boundary of equal free- and bound-drug concentrations is set up by

$$C = S_0 - 1/K \tag{20}$$

which is $C = S_0 - 1/K = 9\mu\text{M}$ for the simulations in this work.

CHAPTER 4

CONCLUSIONS AND FUTURE WORK

4.1 Conclusions

The intravascular drug delivery from a drug-eluting stent and the resulted drug distribution in the arterial wall were modeled. Dimensionless groups were defined that provided insights into the relative importance of directionally-dependent diffusivities and reversible binding on the spatiotemporal distribution of drug in the surrounding arterial wall.

In addition to the drug diffusivities in the coating, the surrounding arterial wall itself greatly influences the release from a drug-eluting stent via the drug diffusivity in the wall and the presence of binding reactions. The findings imply that *in vitro* measurement of release profiles may not be a close representation of the *in vivo* release of a hydrophobic drug from a drug-eluting stent.

Moreover, the average drug concentrations in the arterial wall at quasi-steady state are greatly determined by the drug diffusivity in the wall rather than the drug diffusivity in the stent coating. Anisotropic drug diffusivities in the arterial wall result in similar spatially-averaged drug levels but very different spatial distributions, and higher free-drug concentration than bound-drug concentration can occur at local sites. The critical condition $C_s/\kappa_{CW} > S_0 - 1/K$ (Eq. (19)) for the occurrence of the latter phenomena was derived. Higher circumferential diffusivity reduces the drug gradient in the

circumferential direction and produces more uniformly loaded drug concentrations, which can reduce the thickness of in-stent restenosis after drug-eluting stent treatment.

Simulation results as presented here provide predictions as to how changes in drug properties (such as its directional diffusivity or reversible binding kinetics) influence spatial uniformity in the arterial wall and show potential for guiding the design of drug-eluting stents.

4.2 Future Work

The work of this thesis has been focused on bio-durable polymeric stent coatings in consideration of the available clinical stents in practice. Meanwhile, biodegradable polymers also draws attention in drug-eluting stents coating design due to their favorable biocompatibility compared with bio-durable polymer carriers [46-48]. Commonly studied biodegradable polymers include poly(lactic-*co*-glycolic acid) (PLGA) and poly(lactic acid) (PLA) [49-50].

A unique feature of biodegradable polymeric coating is the degradation of the polymer matrix and resulted change in matrix structure and transport property. The degradation process is recognized as a hydrolysis reaction for PLGA and PLA, where the polymer chains reacts with water molecules and break into smaller segments [50-52]. Drug diffusion within the coating matrix is confined at the beginning due to the very low drug diffusivity in the polymer matrix. As degradation goes, micro pore-structures are being formed within the coating and drug starts to diffuse out through the micro-tunnels built by the pores. The effective drug diffusivity in the coating is a function of the extent

of degradation and this leads to a coupled drug diffusion and polymer degradation process in the coating.

Degradation of PLGA/PLA based microspheres together with drug release has been extensively studied, but there has not been a unanimous mechanistic model that can describe the process precisely [51,53-58]. It has been shown that for PLGA microspheres neither bulk scission nor end scission alone can explain the experimental observation but a combined mechanism of both [58]. More recently, autocatalytic effect has also been proposed to explain accelerated degradation in the interior spheres and models attempt to implement this effect have met quite some complexity [56].

Choosing PLGA (PLA) polymers as our biodegradable coating matrix, the next step of our work is to develop a model to describe and predict the coating matrix degradation and erosion process, which in turn changes the drug release kinetics in the coating. The degradation model can then be incorporated into the established drug transport model to investigate the intravascular drug delivery from a drug-eluting stent with biodegradable coating.

NOMENCLATURE

B	bound drug concentration
C	free drug concentration
C_0	initial drug concentration in the coating
C_s	drug solubility in the coating
D_1	diffusivity in the stent coating
D_2	isotropic diffusivity in the arterial wall
D_{2x}	transmural diffusivity in the arterial wall
D_{2y}	circumferential diffusivity in the arterial wall
h	mesh size
K	binding equilibrium constant, k_a/k_d
k_a	association rate constant
k_d	dissociation rate constant
R	mass transfer resistance
S	available binding sites in the arterial wall
S_0	initial binding sites concentration in the arterial wall
Greek Symbols	
Δt	time step
κ	drug partition coefficient
τ_1	diffusion time scale in the coating
τ_2	diffusion time scale in the arterial wall
τ_3	time scale of drug binding reaction

REFERENCES

[1] M. Santin, P. Colombo, G. Bruschi, Interfacial biology of in-stent restenosis, *Expert Rev. of Med. Devices* 2(4) (2005) 429-443.

[2] R. Fattori, T. Piva, Drug-eluting stents in vascular intervention, *The Lancet* 361(9353) (2003) 247-249.

[3] J.E. Sousa, P.W. Serruys, M.A. Costa, New frontiers in cardiology - Drug-eluting stents: Part I, *Circulation* 107(17) (2003) 2274-2279.

[4] J. Daemen, P.W. Serruys, Drug-eluting stent update 2007 Part I: A survey of current and future generation drug-eluting stents:Meaningful advances or more of the same? *Circulation* 116 (2007) 316-328.

[5] M.A. Costa, D.I. Simon, Molecular basis of restenosis and drug-eluting stents, *Circulation* 111(17) (2005) 2257-2273.

[6] E. Deconinck, J. Sohier, I. De Scheerder, G. Van Den Mooter, Pharmaceutical aspects of drug eluting stents, *J. Pharm. Sci.* 97(12) (2008) 5047-5060.

[7] R. Wessely, A. Schomig, A.Kastrati, Sirolimus and paclitaxel on polymer-based drug-eluting stents: similar but different, *J. Am. Coll. Cardiol.* 47(4) (2006) 708-714.

[8] S.R. Bailey, DES design: Theoretical advantages and disadvantages of stent strut materials, design, thickness, and surface characteristics, *J. Interv. Cardiol.* 22 (2009) S3-S17.

[9] G. Acharya, K. Park, Mechanisms of controlled drug release from drug-eluting stents, *Adv. Drug Deliv. Rev.* 58(3) (2006) 387-401.

[10] S. Venkatraman, F. Boey, Release profiles in drug-eluting stents: Issues and uncertainties, *J. Control. Release* 120(3) (2007) 149-160.

[11] K.R. Kamath, J.J. Barry, K.M. Miller, The taxus (TM) drug-eluting stent: A new paradigm in controlled drug delivery, *Adv. Drug Deliv. Rev.* 58(3) (2006) 412-436.

[12] S.V. Ranade, K.M. Miller, R.E. Richard, A.K. Chan, M.J. Allen, M.N. Helmus, Physical characterization of controlled release of paclitaxel from the TAXUS(TM) express(2TM) drug-eluting stent, *J. Biomed. Mater. Res.* 71A(4) (2004) 625-634.

[13] T. Sharkawi, D. Leyni-Barbaz, N. Chikh, J.N. McMullen, Evaluation of the in vitro drug release from resorbable biocompatible coatings for vascular stents, *J. Bioact. Compatible Polym.* 20(2) (2005) 153-168.

[14] A.D. Levin, N. Vukmirovic, C.W. Hwang, E.R. Edelman, Specific binding to intracellular proteins determines arterial transport properties for rapamycin and paclitaxel, *Proc. Natl. Acad. Sci. USA* 101(25) (2004) 9463-9467.

[15] C.J. Creel, M.A. Lovich, E.R. Edelman, Arterial paclitaxel distribution and deposition, *Circ. Res.* 86(8) (2000) 879-884.

[16] F. Zhang, M. Fath, R. Marks. R.J. Linhardt, A highly stable covalent conjugated heparin biochip for heparin protein interaction studies, *Anal. Biochem.* 304 (2002) 271-273.

[17] C.W. Hwang, E.R. Edelman, Arterial ultrastructure influences transport of locally delivered drugs. *Circ. Res.* 90(7) (2002) 826-832.

[18] A.R.Tzafriri, N.Vukmirovic, V.B. Kolachalama, I. Astafieva, E.R. Edelman, Lesion complexity determines arterial drug distribution after local drug delivery, *J. Control. Release* 142 (3) (2010) 332-338.

[19] C.W. Hwang, A.D. Levin, M. Jonas, P.H. Li, E.R. Edelman, Thrombosis modulates arterial drug distribution for drug-eluting stents, *Circulation* (111) (2005) 1619-1626.

[20] M.A. Lovich, M. Philbrook, S. Sawyer, E. Weselcouch, E.R. Edelman, Arterial heparin deposition: Role of diffusion, convection and extravascular space, *Am. J. Physiol. Heart Circ. Physiol.* 275 (1998) 2236-2242.

[21] M.A. Lovich, E.R. Edelman, Mechanisms of transmural heparin transport in the rat abdominal aorta after local vascular delivery, *Circ. Res.* 77 (1995) 1143-1150.

[22] T. Murata, T. Hiro, T. Fujii, K. Yasumoto, A. Murashige, M. Kohno, J. Yamada, T. Murata, M. Matsuzaki, Impact of the cross-sectional geometry of the post-deployment coronary stent on in-stent neointimal hyperplasia - An intravascular ultrasound study, *Circulation J.* 66(5) (2002) 489-493.

[23] H. Takebayashi, G.S. Mintz, S.G. Carlier, Y. Kobayashi, K. Fujii, T. Yasuda, R.A. Costa, I. Moussa, G.D. Dangas, R. Mehran, A.J. Lansky, E. Kreps, M.B. Collins, A. Colombo, G.W. Stone, M.B. Leon, J.W. Moses, Nonuniform strut distribution correlates with more neointimal hyperplasia after sirolimus-eluting stent implantation, *Circulation* 110(22) (2004) 3430-3434.

[24] A. Finkelstein, D. McClean, S. Kar, K.Takizawa, K. Varghese, N. Baek, K. Park, M. C. Fishbein, R. Makkar, F. Litvack, N. L. Eigler, Local Drug Delivery via a Coronary Stent With Programmable Release Pharmacokinetics, *Circulation* 107 (2003) 777-784.

[25] J.J. Wentzel, R. Krams, J.C.H. Schuurbiers, J.A. Oomen, J. Kloet, W.J. Giessen, P.W. Serruys, C.J. Slager, Relationship between neointimal thickness and shear stress after wallstent implantation in human coronary arteries, *Circulation* 103 (2001) 1740-1745.

[26] S.G. Carlier, L.C.A. Damme, C.P. Blommerde, J.J. Wentzel, G. Langehove, S. Verheye, M.M. Kockx, M.W.M. Knaapen, C. Cheng, F. Gijsen, D.J. Duncker, N. Stergiopulos, C.J. Slager, P.W. Serruys, R. Krams, Augmentation of wall shear stress inhibits neointimal hyperplasia after stent implantation: Inhibition through reduction of inflammation?, *Circulation* 107 (2003) 2741-2746.

[27] S. Hossainy, S. Prabhu, A mathematical model for predicting drug release from a biodurable drug-eluting stent coating, *J. Biomed. Mater. Res.* 87A (2008) 487-493.

[28] M.A. Lovich, E.R. Edelman, Computational simulations of local vascular heparin deposition and distribution, *Am. J. Physiol.* 271 (5) (1996) H2014-H2024.

[29] D.V. Sakharov, L.V. Kalachev, D.C. Rijken, Numerical simulation of local pharmacokinetics of a drug after intravascular delivery with an eluting stent, *J. Drug Targeting* 10 (6) (2002) 507-513.

[30] G. Pontrelli, F. de Monte, A multi-layer porous wall model for coronary drug-eluting stents, *Int J. Heat Mass Transfer* 53 (2010) 3629-3637.

[31] C.W. Hwang, D. Wu, E.R. Edelman, Physiological transport forces govern drug distribution for stent-based delivery, *Circulation* 104 (5) (2001) 600-605.

[32] C.W. Hwang, D. Wu, E. R. Edelman, Impact of transport and drug properties on the local pharmacology of drug-eluting stents, *Acute Cardiac Care* 5 (1) (2003) 7-12.

[33] B. Balakrishnan, J. Dooley, G. Kopia, E.R. Edelman, Thrombus causes fluctuations in arterial drug delivery from intravascular stents, *J. Control. Release* 131 (2008) 173-180.

[34] A. Borghi, E. Foa, R. Balossino, F. Migliavacca, G. Dubini, Modelling drug eluting from stents: Effect of reversible binding in the vascular wall and degradable polymeric matrix, *Comput. Meth. Biomech. Biomed. Eng.* 11 (4) (2008) 367-377.

[35] V.B.Kolachalama, A.R.Tzafriri, D.Y.Arifin, E.R.Edelman, Luminal flow patterns dictate arterial drug deposition in stent-based delivery, *J. Control. Release* 133 (2009) 24-30.

[36] B. Balakrishnan, J.F. Dooley, G. Kopia, E.R. Edelman, Intravascular drug release kinetics dictate arterial drug deposition, retention, and distribution, *J. Control. Release* 123 (2) (2007) 100-108.

[37] B. Balakrishnan, A.R. Tzafriri, P. Seifert, A. Groothuis, C. Rogers, E.R. Edelman, Strut position, blood flow, and drug deposition - Implications for single and overlapping drug-eluting stents, *Circulation* 111 (22) (2005) 2958-2965.

[38] M. Grassi, G. Pontrelli, L. Teresi, G. Grassi, L. Comel, A. Ferluga, L. Galasso, Novel design of drug delivery in stented artery: a numerical comparative study, *Math. Bio. & Eng.* 6 (3) (2009) 493-508.

[39] R. Mongrain, I. Faik, R.L. Leask, J. Rodes-Cabau, E. Larose, O.F. Bertrand, Effects of diffusion coefficients and struts apposition using numerical simulations for drug eluting coronary stents, *J. Biomech. Eng.* 129 (5) (2007) 733-742.

[40] G. Vairo, M. Cioffi, R.Cottone, G.Dubini, F. Migliavacca, Drug release from coronary eluting stents: A multidomain approach, *J. Biomech.* 43 (2010) 1580-1589.

[41] R. Mongrain, R. Leask, J.Brunette, I.Faik, N.Bulman-Feleming, T.Nguyen, Numerical modeling of coronary drug eluting stents, *Studies in Health Technology and Informatics* 113 (2005) 443-458.

[42] P. Zunino, C. D'Angelo, L.Petrini, C.Vergara, C.Capelli, F. Migliavacca, Numerical simulation of drug eluting coronary stents: Mechanics, fluid dynamics and drug release, *Comput. Methods Appl. Mech. Engrg.* 198 (2009) 3633-3644.

[43] P. Mortier, G.A. Holzapfel, M. De Beule, D.V. Loo, Y. Taeymans, P. Segers, P. Verdonck, B. Verhegghe, A novel simulation strategy for stent insertion and deployment in curved coronary bifurcations: comparison of three drug-eluting stents, *Ann. Biomed. Eng.* 38 (1) (2010) 88-99.

[44] G. Baroldi, R. Bigi, L. Cortigiani, Ultrasound imaging versus morphopathology in cardiovascular diseases. *Coronary atherosclerotic plaque, Cardiovascular Ultrasound* 2 (2004) 29.

[45] D.S. Cohen, T. Erneux, Controlled drug release asymptotics, *SIAM J.Appl.Math.* 58(4) (1998) 1193-1204.

[46] C.J. Pan, J.J. Tang, Y.J. Weng, J. Wang, N. Huang, Preparation and in vitro release profiles of drug-eluting controlled biodegradable polymer coating stents, *Colloids and Surfaces B: Biointerfaces* 73 (2009) 199-206.

[47] M. Kamberi, S. Nayak, K. Myo-Min, T.P. Carter, L. Hancock, D. Feder, A novel accelerated in vitro release method for biodegradable coating of drug eluting stents: Insight to the drug release mechanisms, *European J. of Pharm. Sci.* 37 (2009) 217-222.

[48] X. Wang, S. S. Venkatraman, F.Y.C. Boey, J.S.C. Loo, L. P. Tan, Controlled release of sirolimus from a multilayered PLGA stent matrix, *Biomaterials* 27 (32) (2006) 5588-5595.

[49] A.G. Hausberger, P.P. DeLuca, Characterization of biodegradable poly(D,L-lactide-co-glycolide) polymers and microspheres, *J. Pharm. Biomed. Anal.* 13 (6) (1995) 747-760.

[50] U. Edlund, A. -C. Albertsson, Degradable polymer microspheres for controlled drug delivery, *Adv. Polymer Sci.* vol 157/2000 (2002) 67-112.

[51] F. von Burkersroda, L. Schedl, A. Göpferich, Why degradable polymers undergo surface erosion or bulk erosion, *Biomaterials* 23 (21) (2002) 4221-4231.

[52] S. Freiberg, X. X. Zhu, Polymer microspheres for controlled drug release, *Int. J. Pharm.* 282 (2004) 1-18.

[53] A. Charlier, B. Leclerc, G. Couarraze, Release of mifepristone from biodegradable matrices: experimental and theoretical evaluations, *Int. J. Pharm.* 200 (1) (2000) 115-120.

[54] D. Larobina, G. Mensitieri, M.J. Kipper, B. Narasimhan, Mechanistic understanding of degradation in bioerodible polymers for drug delivery, *AIChE J.* 48 (2002) 2960-2970.

[55] B. S. Zolnik, D.J. Burgess, Effect of acidic pH on PLGA microsphere degradation and release, *J. Control. Release* 122 (3) (2007) 338-344.

[56] D. Klose, F. Siepmann, K. Elkharraz, S. Krenzlin, J. Siepmann, How porosity and size affect the drug release mechanisms from PLGA-based microparticles, *Int. J. Pharm.* 314 (2) (2006) 198-206.

[57] C. Raman, C. Berkland, K. Kim, D. W. Pack, Modeling small-molecule release from PLG microspheres: effects of polymer degradation and nonuniform drug distribution, *J. Control. Release* 103 (1) (2005) 149-158.

[58] R. P. Batychy, J. Hanes, R. Langer, D.A. Edwards, A theoretical model of erosion and macromolecular drug release from biodegrading microspheres, *J. Pharm. Sci.* 86 (12) (1997) 1464-1477.

APPENDIX A

SIMULATION VERIFICATION BY ANALYTICAL SOLUTION IN 1–D CASE

A.1 Introduction

The verification of the Matlab program code is completed by comparing the simulation results to analytical solutions. In order to acquire a feasible analytical solution, high drug loading case (continuum pharmacokinetics) is investigated (detail descriptions of high drug loading case can be referred to in Chapter 3). A zero value of circumferential diffusivity reduces the problem to a one-dimensional (1–D) case.

A.2 Analytical Solution of Continuum Pharmacokinetics in 1–D

At high drug loading in the stent coating, the free and bound drug concentrations in the arterial wall achieve quasi-equilibrium levels before the drug aggregates are depleted in the coating.

Under quasi-equilibrium state, the drug concentrations in the wall are described by a set of ordinary differential equations, Eqs. A (1) and A (2).

For free drug in the arterial wall,

$$\frac{d^2C}{dx^2} = 0 \qquad \text{A (1)}$$

For bound drug in the arterial wall,

$$\frac{dB}{dt} = k_a C(S_0 - B) - k_d B = 0 \qquad \text{A (2)}$$

The boundary conditions at the coating-arterial wall interface and perivascular boundary are described in Eqs. A (3) and A (4), respectively.

$$C = C_S \qquad \text{A (3)}$$

$$J\Big|_{peri} = \frac{1}{R_{wp}}(C_{peri} - \frac{C_{wall}}{\kappa_{wp}}) \qquad \text{A (4)}$$

Substitute values from Table 1 and solve the ODEs to get the analytical solutions:

Free drug in the arterial wall

$$C = -\frac{C_S}{R_{per} D_{2x} + L}(x - L) + C_S \qquad \text{A (5)}$$

Bound drug in the arterial wall

$$B = \frac{k_a C S_0}{k_a C + k_d} \qquad \text{A (6)}$$

A.3 Simulation Results Compared With Analytical Solution

Simulation of the same parameters gives identical results as the analytical solution (Eqs. A (5) & A (6), as shown in Figure A1. This confirms the validity of the Matlab code for this model.

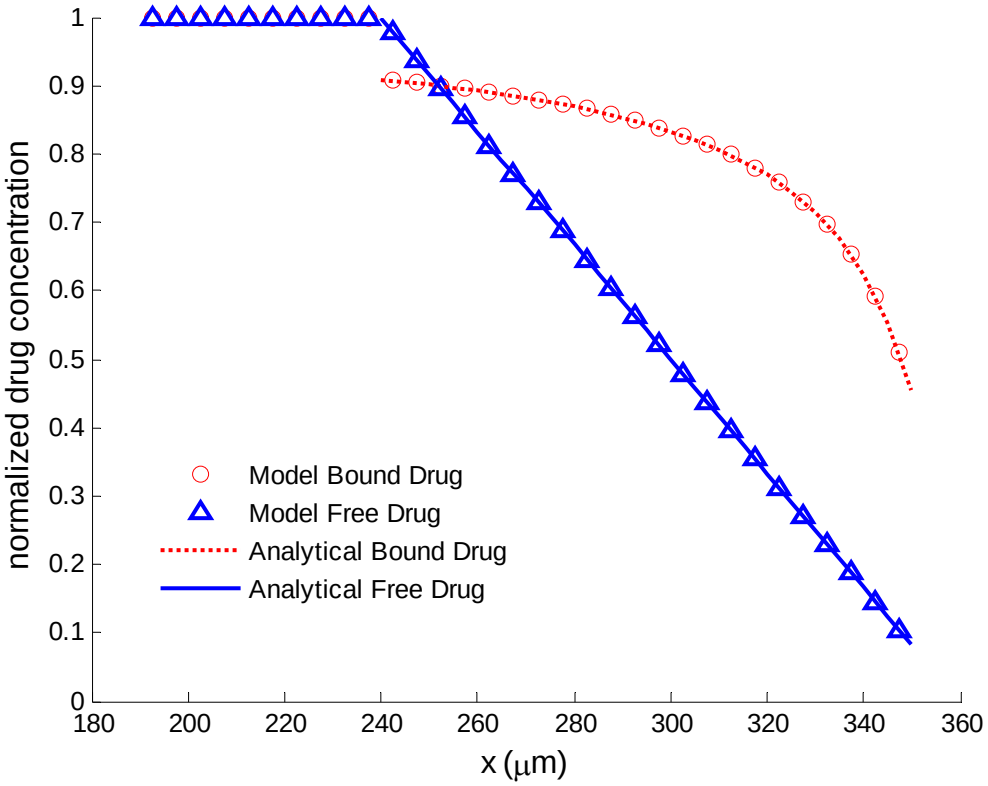

Figure A1. Free and bound drug concentrations in the arterial wall at quasi-equilibrium in the test case. Coating-arterial interface starts at $x = 240$ μm.